DOI: 10.1021/ic1006567

Inorganic Chemistry
Article

Separation of Geometric Isomers of a Dicopper Complex by Using a ^{19}F-Labeled Ligand: Dynamics, Structures, and DFT Calculations

Stéphanie Durot,[†] Laila H. Hossain,[†] Sylvain Hamman,[†] Hélène Jamet,[†] Maylis Orio,[†] Isabelle Gautier-Luneau,[‡] Dominique Luneau,[§] Christian Philouze,[†] Jean-Louis Pierre,[†] and Catherine Belle*[,†]

[†]*Département de Chimie Moléculaire, Université Joseph Fourier, équipes CIRE et Chimie Théorique UMR-CNRS 5250, ICMG FR-2607, BP 53, 38041 Grenoble Cedex 9, France,* [‡]*Institut Néel, Université Joseph Fourier, CNRS, UPR 2940, 25 rue des Martyrs, BP 166, 38042 Grenoble Cedex 9, France, and* [§]*Laboratoire des Multimatéraux et Interfaces, Université Claude Bernard, UMR-CNRS 5615, campus de la Doua, 69622 Villeurbanne Cedex, France*

Received April 7, 2010

Introducing a fluorine group on two pyridines of the HL_{CH_3} ligand (2,6-bis[(bis(2-pyridylmethyl)amino)methyl]-4-methylphenol) allows the separation of two geometric isomers after complexation by two copper(II) ions. Methods for isolating the isomers ($\mathbf{1_{meso}}$ and $\mathbf{1_{rac}}$) as a μ-phenoxo,μ-hydroxo dicopper(II) complex as a crystalline product have been developed. Both isomers ($\mathbf{1_{meso}}$ and $\mathbf{1_{rac}}$) have been characterized by X-ray crystallography and ^{19}F NMR. The isomerism is determined by the disposition of the fluorine atoms with respect to the plane containing the Cu_2O_2 core. Density functional theory calculations using different functionals were performed to provide additional support for the existence of these two forms. Dissolution of $\mathbf{1_{meso}}$ in acetone or acetonitrile causes its spontaneous isomerization into the $\mathbf{1_{rac}}$ form at room temperature. Combined experimental studies (UV−vis, ^{19}F NMR) and theoretical calculations support this process. Paramagnetic ^{19}F NMR appears as a unique and powerful probe for distinguishing the two isomers and supplying direct evidence of this isomerization process in solution.

Introduction

Dinuclear metal complexes supported by 2,6-bis[(bis(2-pyridylmethyl)amino)methyl]-4-methylphenol-type ligands[1−4] (Scheme 1a) have received a great deal of attention from the scientific community in recent decades. The interest in these types of compounds is to a large extent due to their ability to assemble bimetallic complexes that model the properties of metalloprotein active sites. In particular, dinuclear iron, copper, zinc, or nickel structures involving metal−metal separations ranging from 3.0 to 4.0 Å have been reported[5−12] and representatives examples reviewed.[13,14] As part of our interest in model compounds for the type-3 active site of copper proteins,[15] we prepared and structurally characterized dinuclear copper(II) complexes with this type of ligand.[16,17] In these complexes, two copper ions are kept together by the phenoxo moiety, each copper ion surrounded by three nitrogen donor atoms from the ligand. In addition, the copper(II) ions are bridged by an exogenous hydroxo group. The structure of the complexes are thus fairly similar to the *met*-form of the active site of catechol oxidase and tyrosinase, consisting of two copper(II) centers, each linked with three histidine residues and a hydroxo bridge.[18−21] The investigation of the catalytic properties of

*E-mail: catherine.belle@ujf-grenoble.fr. Phone: +33-476514838. Fax: +33-476514836.

(1) Suzuki, M.; Kanatomi, H.; Murase, I. *Chem. Lett.* **1981**, 1745.
(2) Borovick, A. S.; Papaefthymiou, V.; Taylor, H. V.; Anderson, B. F.; Que, L., Jr. *J. Am. Chem. Soc.* **1989**, *111*, 6183.
(3) Vigato, P. A.; Tamburini, S. *Coord. Chem. Rev.* **2008**, *252*, 1871.
(4) Gavrilova, A. L.; Bosnich, B. *Chem. Rev.* **2004**, *104*, 349.
(5) Schepers, K.; Bremer, B.; Krebs, B.; Henkel, G.; Althaus, E.; Mosel, B.; Müller-Warmuth, W. *Angew. Chem., Int. Ed. Engl.* **1990**, *29*, 531.
(6) Karlin, K. D.; Cruse, R. W.; Gultneh, Y.; Farooq, A.; Hayes, J. C.; Zubieta, J. *J. Am. Chem. Soc.* **1987**, *109*, 2668.
(7) Borovick, A. S.; Hendrich, M. P.; Holman, T. R.; Münck, E.; Papaefthymiou, V.; Que, L., Jr. *J. Am. Chem. Soc.* **1990**, *112*, 6031.
(8) Suzuki, M.; Kanatomi, H.; Murase, I. *Bull. Chem. Soc. Jpn.* **1984**, *57*, 36.
(9) Adams, H. A.; Bradshaw, D.; Fenton, D. E. *Inorg. Chim. Acta* **2002**, *332*, 195.
(10) Shiraishi, H.; Jikido, R.; Matsufuji, K.; Nakanishi, T.; Shiga, T.; Ohba, M.; Sakai, K.; Kitagawa, H.; Okawa, H. *Bull. Chem. Soc. Jpn.* **2005**, *78*, 1072.
(11) Albedyhl, S.; Averbuch Pouchot, M. T.; Belle, C.; Krebs, B.; Pierre, J. L.; Saint Aman, E.; Torelli, S. *Eur. J. Inorg. Chem.* **2001**, *6*, 1457.
(12) Selmeczi, K.; Michel, C.; Milet, A.; Gautier-Luneau, I.; Philouze, C.; Pierre, J. L.; Schnieders, D.; Rompel, A.; Belle, C. *Chem. Eur. J.* **2007**, 9093.
(13) Suzuki, M.; Furutachi, H.; Okawa, H. *Coord. Chem. Rev.* **2000**, *200−202*, 105.
(14) Gahan, J. R.; Smith, S. J.; Neves, A.; Schenk, G. *Eur. J. Inorg. Chem.* **2009**, *19*, 2735.
(15) Solomon, E. I.; Sudaram, U. M.; Mackonkin, T. E. *Chem. Rev.* **1996**, *96*, 2563–2605.
(16) Torelli, S.; Belle, C.; Gautier Luneau, I.; Pierre, J. L.; Saint Aman, E.; Latour, J. M.; Le Pape, L.; Luneau, D. *Inorg. Chem.* **2000**, *39*, 3526.
(17) Torelli, S.; Belle, C.; Gautier-Luneau, I.; Hamman, S.; Pierre, J. L. *Inorg. Chim. Acta* **2002**, *333*, 144.
(18) Klabunde, T.; Eicken, C.; Sacchettini, J. C.; Krebs, B. *Nat. Struct. Biol.* **1998**, *5*, 1084.

Published on Web 08/12/2010

Scheme 1. Dinucleating Phenol-Based Ligands Included in This Work: (a) From Refs 16 and 30; (b) $F_2-HL_{CH_3}$ Ligand Described in This Work

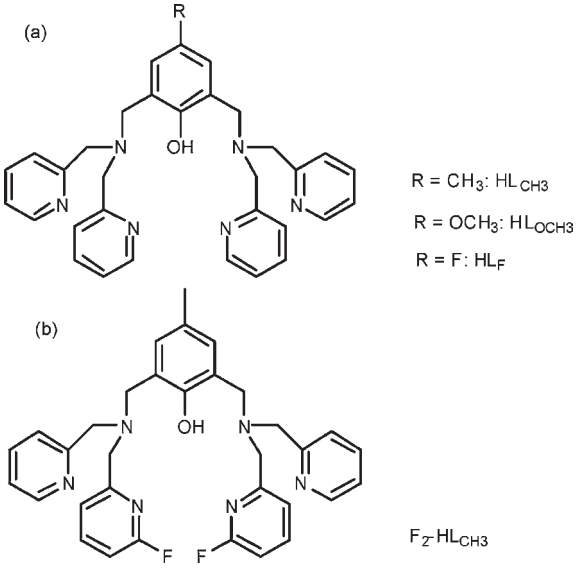

such model complexes would provide more insight into the structure/activity relationship.[22] This interest is driven by the search for the right balance between the steric and electronic demands of the ligand to optimize the observed catalytic activity, i.e., oxidation of model catechol substrates to the corresponding quinones. Furthermore, the reactivity of a such dicopper(II) center model can be probed using substrates and inhibitors of copper protein type-3 active sites.[23]

Various dinuclear metal complexes supported by diaminomethylated phenol-based symmetric ligands having mixed pyridine and substituted pyridine or phenolate pendant arms have been described.[24−26] To the best of our knowledge, only studies performed on zinc complexes have mentioned that geometric isomeric complexes could be potentially obtained (observed on diamagnetic ^{1}H NMR spectrum).[27,28] Unfortunately, no X-ray structures of both isomeric forms have been reported.

Our investigations in this field led us to consider partially fluorinated species. We describe in this paper a dinucleating phenol-based ligand F_2-HL_{CH_3} (Scheme 1b) with pendant pyridine arms, two of them bearing a fluorine group. F is introduced into the ligand to study the possible geometric isomers on corresponding dinuclear copper complexes. Furthermore, the presence of fluorine enables us to use ^{19}F NMR as a probe of the spatial arrangement of endogen ligands. This 100% abundant spin-1/2 nucleus, with high sensitivity, spectral simplicity, and large chemical shift, is particularly attractive for paramagnetic systems in the field of bioinorganic chemistry (proteins and models).[29] The potential applicability of paramagnetic ^{19}F NMR to models complexes described herein or in previous publications can give valuable information in terms of observation of possible isomers, solution equilibria, coordination changes as a function of pH,[30] investigation of substrate or inhibitor binding,[23,30] and spatial interactions of substrates with paramagnetic centers and identification of reactions intermediates.[31] This information is of great importance for understanding the observed catalytic processes, i.e., oxidation of model catechol substrates to the corresponding quinones in relation to catechol oxidation by copper protein type-3 active sites (tyrosinase and catechol oxidase).

Ligand synthesis and complex characterization of $[Cu_2(F_2\text{-}L_{CH_3})(\mu\text{-}OH)](ClO_4)_2$ are presented and compared to the previously investigated complexes with related monofluorinated and nonfluorinated ligands (Scheme 1): $[Cu_2(L_F)(\mu\text{-}OH)](ClO_4)_2$[30] and $[Cu_2(L_{CH_3})(\mu\text{-}OH)](ClO_4)_2\cdot 0.5C_4H_8O$,[16] respectively.

Furthermore, the electronic structures of dinuclear copper(II) complexes remain a theoretical challenge due to the difficulty of providing an accurate description of electron correlation effects for these systems.[32−36] The availability of X-ray structures for both isomeric forms allows us to check the validity of a wide range of theoretical models. In this context, density functional theory (DFT) calculations were performed and compared to experimental results.

Experimental Section

General. All reagents were purchased from commercial sources and used as received. Solvents were purified by standard methods before use.

Caution! *Although no problems were encountered in this work, suitable care and precautions should be taken when handling perchlorate salts.*

Elemental analyses were performed by the CNRS Microanalysis Laboratory (Lyon, France). Mass spectra were obtained with a Nermag R 1010C apparatus equipped with an M scan (Wallis) atom gun (8 kV, 20 mA) with fast-atom bombardment (FAB) ionization in the positive mode. Electrospray ionization (ESI) mass spectra were recorded on an Esquire 300 plus Bruker Daltonis or ZQ 2000 instrument, using MK II Z-spray from Waters fitted with a syringe pump. UV−vis spectra were obtained using a Cary 50 spectrophotometer operating in the 200−1000 nm range with quartz cells. The temperature was maintained at 25 °C with a temperature control unit. ^{1}H NMR spectra were recorded on a Bruker AC 200 or Bruker Advance 300 spectrometer at 323 K with the deuterated solvent as a lock. ^{19}F NMR experiments were carried out on a Bruker Advance 300 spectrometer at 323 K, where the ^{19}F resonance frequency was 282.395 MHz. Chemical shifts in ppm are given relative to

(19) Volbeda, A.; Hol, W. G. *J. Mol. Biol.* **1989**, *209*, 249.
(20) Volbeda, A.; Hol, W. G. *J. Mol. Biol.* **1989**, *206*, 531.
(21) Matoba, Y.; Kumagai, T.; Yamamoto, A.; Yoshitsu, H.; Sugiyama, M. *J. Biol. Chem.* **2006**, *281*, 8981.
(22) Koval, I. A.; Gamez, P.; Belle, C.; Selmeczi, K.; Reedijk, J. *Chem. Soc. Rev.* **2006**, *35*, 814.
(23) Peyroux, E.; Ghattas, W.; Hardré, R.; Giorgi, M.; Faure, B.; Simaan, A. J.; Belle, C.; Réglier, M. *Inorg. Chem.* **2009**, *48*, 10874.
(24) Krebs, B.; Schepers, K.; Bremer, B.; Henkel, G.; Althaus, E.; Müller-Warmuth, W.; Griesar, K.; Haase, W. *Inorg. Chem.* **1994**, *33*, 1907.
(25) Koval, I. A.; Huisman, M.; Stassen, A. F.; Gamez, P.; Roubeau, O.; Belle, C.; Pierre, J. L.; Saint Aman, E.; Lüken, M.; Krebs, B.; Lutz, M.; Spek, A. L.; Reedijk, J. *Eur. J. Inorg. Chem.* **2004**, 4036.
(26) Amudha, P.; Kandaswamy, M.; Govindasamy, L.; Velmurugan, D. *Inorg. Chem.* **1998**, *37*, 4486.
(27) Williams, C. K.; Brooks, N. R.; Hillmyer, M. A.; Tolman, W. *Chem. Commun.* **2002**, 2132.
(28) Kaminskaia, N. V.; Spingler, B.; Lippard, S. J. *J. Am. Chem. Soc.* **2000**, *122*, 6411.
(29) Belle, C.; Béguin, C.; Hamman, S.; Pierre, J.-L. *Coord. Chem. Rev.* **2009**, *253*, 963.
(30) Belle, C.; Béguin, C.; Gautier-Luneau, I.; Hamman, S.; Philouze, C.; Pierre, J. L.; Thomas, F.; Torelli, S. *Inorg. Chem.* **2002**, *41*, 479.
(31) Torelli, S.; Belle, C.; Hamman, S.; Pierre, J. L.; Saint Aman, E. *Inorg. Chem.* **2002**, *41*, 3983.
(32) Flock, M.; Pierloot, K. *J. Phys. Chem. A* **1999**, *103*, 95.
(33) Eisenstein, O.; Getlicherman, H.; Giessner-Prettre, C.; Maddaluno, J. *Inorg. Chem.* **1997**, *36*, 3455.
(34) Lind, T.; Siegbahn, P. E. M. *Faraday Discuss.* **2003**, *124*, 289.
(35) Cramer, M.; Wloch, P.; Piecuch, C.; Puzzarini, L.; Gagliardi, L. *J. Phys. Chem. A* **2006**, *110*, 1991.
(36) Piquemal, J.-P.; Pilme, J. *J. Mol. Struct.: THEOCHEM* **2006**, *764*, 77.

C_6F_6 used as an external reference (δ C_6F_6 = −162.17 ppm vs $CFCl_3$). A typical spectrum consisted of 32K data points, 1000 scans on a 28-kHz bandwidth, and a 100-ms relaxation delay. An exponential weighting function (LB = 20 Hz) was used during the processing.

Synthesis. 2-Fluoro-6-(dibromomethyl)pyridine (2). A 5-g (45 mmol) portion of commercially available 2-fluoro-6-methylpyridine was dissolved in 400 mL of CCl_4. A 16-g (90 mmol) portion of *N*-bromosuccinimide (NBS) was added, and the medium was refluxed for 24 h in the presence of 100 mg of benzoyl peroxide. An additional amount (100 mg, 4 mmol) of benzoyl peroxide was added, and the mixture was refluxed for 30 h. The solvent was then evaporated, and the crude compound was purified by silica gel chromatography using hexane/ethyl acetate (9/1) as eluent. Evaporation of the solvent gave **2** (9.2 g, 75%) as a pale yellow oil: δ_H (300 MHz, $CDCl_3$) 7.92 (1H, q, $^3J_{HH}$ 10.9, $^3J_{HF}$ 7.5, $^4J_{HF}$ 8.0, CH-C*H*-CH), 7.66 (1H, dd, $^3J_{HH}$ 7.1, $^3J_{HH}$ 2.7, -C*H*-C-$CHBr_2$), 6.92 (1H, dd, $^3J_{HH}$ 10.9, $^4J_{HF}$ 2.7, -C*H*-CF), 6.59 (1H, s, C*H*Br_2); δ_F (282.395 MHz, $CDCl_3$, C_6F_6) 95.97 (s, Py-F).

6-Fluoro-2-pyridinecarboxaldehyde (3). $AgNO_3$ (10 g, 59 mmol), dissolved in 10 mL of distilled water, was added drop by drop to a solution of dibrominated species **2** (4.0 g, 15 mmol) dissolved in 3 mL of acetonitrile. After 3 h, brine solution was added to precipitate excess silver ions. The suspension was then filtrated over Celite deposited on a glass frit, and the aqueous layer of the filtrate was extracted with dichloromethane (5 × 20 mL). The combined organic layers were carefully concentrated under reduced pressure to give a crude product (without heating, low boiling point). Distillation (65 °C) gave **3** as a clear oil (1,1 g, 60%): δ_H (300 MHz, $CDCl_3$) 9.96 (1H, s, C*H*O), 8.01 (1H, q, $^3J_{HH}$ 7.9, $^3J_{HH}$ 7.5, $^4J_{HF}$ 8.0, CH-C*H*-CH), 7.87 (1H, dd, $^3J_{HH}$ 7.5, $^5J_{HF}$ 1.7, -C*H*-C-CHO), 7.24 (1H, dd, $^3J_{HH}$ 7.9, $^3J_{HF}$ 2.4, -C*H*-CF); δ_F (282.395 MHz, $CDCl_3$, C_6F_6) 95.8 (s, Py-F).

***N*-(2-Pyridylmethyl),*N*′-(6-fluoro-2-pyridinemethyl)amine (4).** To a solution of **3** (438 mg, 3.5 mmol) in dry methanol (4 mL) was added 2-(aminomethyl)pyridine (367 mg, 3.4 mmol) in dry methanol (5 mL) at room temperature under an inert atmosphere of nitrogen. After 2 h, $NaBH_4$ (358 mg, 9.5 mmol) was slowly added as a solid, and the mixture was stirred for an additional 3.5 h. After acidic treatment (4 N HCl) to pH 1, the solvent was removed under reduced pressure. The resulting product was dissolved in water (100 mL) and washed with dichloromethane. The aqueous solution was then neutralized with saturated $NaHCO_3$ until pH 8 and extracted with dichloromethane (2 × 100 mL). The combined organic layers were washed with saturated NaCl, dried over Na_2SO_4, and concentrated under reduced pressure to give a yellow oil (860 mg, 82%), which was used without further purification: δ_H (300 MHz, $CDCl_3$, Me_4Si) 8.56 (1H, d, $^3J_{HH}$ 4.7, C*H*-N), 7.73 (1H, q, $^3J_{HH}$ 8.2, $^3J_{HH}$ 7.3, $^4J_{HF}$ 8.0, FC-CH-C*H*-), 7.6 (1H, m, C-CH-C*H*-CH), 7.34 (1H, m, CH-C*H*-C-N), 7.26 (1H, dd, $^3J_{HH}$ 7.3, $^5J_{HF}$ 2.6, -C*H*-CH-CH-CF), 7.14 (1H, m, -C*H*-CH-N), 6.77 (1H, dd, $^3J_{HH}$ 8.2, $^3J_{HF}$ 2.6, -C*H*-CF-), 3.97 (2H, s, -CH_2-Py-F), 3.93 (2H, s, -CH_2-Py), 2.41 (1H, s, N*H*); δ_F (282.395 MHz, $CDCl_3$, C_6F_6) 94.1 (s, Py-F).

F_2-HL_{CH_3}. Under a dinitrogen atmosphere, a mixture of amine **4** (382 mg, 1.8 mmol) and triethylamine (494 μL, 3.5 mmol) in 8 mL of dry tetrahydrofuran (THF) was added dropwise to a stirred solution of 2,6-bis(chloromethyl)-4-methylphenol (179 mg, 0.9 mmol) in 9 mL of dry THF at 0 °C. When the addition was completed, the resulting mixture was allowed to warm to room temperature. After 2.5 days, the resulting mixture was filtered, and the filtrate was concentrated under reduced pressure. The residue was dissolved in 100 mL of methylene chloride, washed with brine, and dried over anhydrous Na_2SO_4. The solution was evaporated to dryness under reduced pressure, and a crude product was obtained as a brown oil. Chromatography on silica gel using ethyl acetate was performed, and the desired compound was collected. Evaporation of the solvent yielded 179 mg (30%) of pure F_2-HL_{CH_3} as a brown oil: δ_H (300 MHz, $CDCl_3$, Me_4Si) 8.55−8.53 (2H, m, C*H*-N), 7.76−7.60 (4H, m, -C*H*-CH-CF and -C*H*-CH-CH-N), 7.48−7.40 (4H, m, N-CH-C*H*- and -FC-N-C-C*H*-), 7.17−7.12 (2H, m, CH-N-C-C*H*-), 6.97 (2H, s, Me-C-C*H*-), 6.75 (2H, dd, $^3J_{HH}$ 3.6, $^3J_{HF}$ 7.9, -C*H*-CF-), 3.89 (4H, s, N-CH_2-Py-F), 3.80 (4H, s, N-CH_2-Py), 3.78 (4H, s, Ph-CH_2-N), 2.23 (3H, s, Me); δ_F (282.395 MHz, acetone-d_6, C_6F_6) 93.7 (s, py-F); *m*/*z* (DCI) 567 (M + H^+ (100%); $C_{33}F_2H_{32}N_6O$ requires 566). Elemental analysis for $C_{33}H_{32}F_2ON_6 \cdot 0.5CH_3COOCH_2CH_3$, calcd: C, 68.84; H, 5.94; N, 13.76. Found: C, 68.38; H, 5.21; N, 13.43.

Complex 1: $[Cu_2(F_2\text{-}L_{CH_3})(OH)][ClO_4]_2$. To 60 mg (0.106 mmol) of F_2-HL_{CH_3} dissolved in CH_3CN (1.5 mL) was added a solution of 76 mg of $Cu(ClO_4)_2 \cdot 6H_2O$ (0.206 mmol) in CH_3CN (0.5 mL). The initial yellow solution turned brown and was stirred for 10 min at room temperature. Next 44 μL (0.31 mmol) of Et_3N was added, and the solution, which turned dark green, was stirred for 30 min at room temperature. The solvent was partially removed under reduced pressure, and after addition of some amount of THF, the resulting solution was allowed to stand overnight at −20 °C. Afterward, 22 mg of a green powder was collected by filtration: EPR silent (frozen solution of CH_3CN/DMSO 1:1 at 100 K, 3 mM).

$1_{meso} \cdot 3C_4H_8O$. Crystals of X-ray quality were obtained at −20 °C in 2 days in a CH_3CN/THF solution of **1**. The crystalline material, when crushed and exposed to air, loses some non-coordinated THF. Elemental analysis for $C_{33}H_{32}F_2O_2N_6Cu_2 \cdot (ClO_4)_2 \cdot 0.5C_4H_8O$, calcd: C, 44.50; H, 3.84; N, 8.90. Found: C, 44.56; H, 4.01; N, 8.68.

$1_{rac} \cdot CH_3CN$. Crystals of X-ray quality were obtained after 6 weeks by slow evaporation of a CH_3CN/H_2O (1/1) solution of **1**. The crystalline material, when crushed and exposed to air, loses non-coordinated CH_3CN. Elemental analysis for $C_{33}H_{32}F_2O_2N_6Cu_2 \cdot (ClO_4)_2$, calcd: C, 43.63; H, 3.55; N, 9.25. Found: C, 43.74; H, 3.87; N, 8.95.

Crystal Structure Determination and Refinement. Single crystals of complexes $1_{meso} \cdot 3C_4H_8O$ and $1_{rac} \cdot CH_3CN$ were mounted on a Nonius Kappa CCD diffractometer equipped with graphite-monochromated Mo Kα radiation (λ = 0.71073 Å) at 150 K. The reflections were corrected for Lorentz and polarization effects but not for absorption. The structures were solved by direct methods and refined using TEXSAN software.[37] For both structures, all non-hydrogen atoms were refined with anisotropic thermal parameters. Hydrogen atoms were generated in idealized positions, riding on the carrier atoms, with isotropic thermal parameters, except for the hydrogen atom of the hydroxyl group, which was localized on a difference Fourier map and was added. It was refined riding on the carrier atoms with isotropic thermal parameters.

The CCDC reference numbers are 693925 and 724449 for $1_{meso} \cdot 3C_4H_8O$ and $1_{rac} \cdot CH_3CN$, respectively. Pertinent crystallographic data and refinement details are summarized in Table 1.

Computational Methods. Spin-unrestricted DFT calculations were performed with the Gaussian03 software package.[38]

(37) *TEXSAN*, Single Crystal Structure Analysis Software, Version 1.7; Molecular Structure Corp.: The Woodlands, TX, 1995.

(38) Frisch, M. J.; Trucks, G. W.; Schlegel, H. B.; Scuseria, G. E.; Robb, M. A.; Cheeseman, J. R.; Zakrzewski, V. G.; Montgomery, J. A.; Stratmann, J. R. E.; Burant, J. C.; Dapprich, S.; Millam, J. M.; Daniels, A. D.; Kudin, K. N.; Strain, M. C.; Farkas, O.; Tomasi, J.; Barone, V.; Cossi, M.; Cammi, R.; Mennucci, B.; Pomelli, C.; Adamo, C.; Clifford, S.; Ochterski, J.; Petersson, G.; Ayala, A. P. Y.; Cui, Q.; Morokuma, K.; Malick, D. K.; Rabuck, A. D.; Raghavachari, K.; Foresman, J. B.; Cioslowski, J.; Ortiz, J. V.; Baboul, A. G.; Stefanov, B. B.; Liu, G.; Liashenko, A.; Piskorz, P.; Komaromi, I.; Gomperts, R.; Martin, R. L.; Fox, D. J.; Keith, T.; Al-Laham, M. A.; Peng, C. Y.; Nanayakkara, A.; Challacombe, M.; Gill, P. M. W.; Johnson, B.; Chen, W.; Wong, M. W.; Andres, J. L.; Gonzalez, C.; Head-Gordon, M.; Pople, J. A. *Gaussian03*, Revision A1.1; Gaussian Inc.: Pittsburgh, PA, 2003.

Table 1. Crystallographic and Refinement Details for $\mathbf{1}_{meso}$ and $\mathbf{1}_{rac}$

	$\mathbf{1}_{meso}\cdot 3C_4H_8O$ (from CH_3CN/THF)	$\mathbf{1}_{rac}\cdot CH_3CN$ (from CH_3CN/H_2O)
formula	$[Cu_2(C_{33}H_{31}F_2ON_6)(OH)](ClO_4)_2\cdot 3C_4H_8O$	$[Cu_2(C_{33}H_{31}F_2ON_6)(OH)](ClO_4)_2\cdot CH_3CN$
fw	1124.96	968.00
morphology	green prism	dark green fragment
crystal size	$0.30 \times 0.20 \times 0.15$ mm	$0.38 \times 0.35 \times 0.33$ mm
crystal system	triclinic	triclinic
space group	$P\bar{1}$	$P\bar{1}$
a (Å)	12.256(1)	9.871(2)
b (Å)	12.361(3)	12.021(2)
c (Å)	17.571(2)	17.340(4)
α (°)	107.87(2)	104.82(1)
β (°)	102.88(2)	100.22(2)
γ (°)	94.30(2)	92.55(2)
unit-cell volume (Å^3)	2440.1(7)	1948.8(7)
D_x (g cm^{-3})	1.53	1.618
T (K)	150	150
Z	2	2
μ (mm^{-1})	1.058	1.304
total reflections	50 280	28 474
unique reflections	13 329	6759
obsd reflections	7456 ($F > 2\sigma$)	4933 ($F > 2\sigma$)
R_{int}	0.078	0.044
R^a	0.055	0.045
R(w)^a	0.069	0.055
goodness of fit, S	1.93	1.69
$\Delta\rho_{min}/\Delta\rho_{max}$ (e Å^{-3})	−0.5/1.37	−0.40/0.54

[a] Refinement based on F where $w = 1/[\sigma^2(F) + 0.00038|F_o|^2]$ for $\mathbf{1}_{meso}$ and $w = 1/[\sigma^2(F) + 0.00027|F_o|^2]$ for $\mathbf{1}_{rac}$.

All geometry optimizations were carried out in the gas phase using the BLYP functional[39,40] together with the 6-31g* basis set for all atoms on both triplet ($S = 1$) and broken-symmetry ($M_s = 0$) states. For the broken-symmetry state, a single-point calculation was performed using the high-spin wave function and the guess = (read, mix) keyword to generate the unrestricted broken-symmetry singlet wave function before the geometry optimization. Vibrational frequency calculations were performed to ensure that each geometry optimization converged to a real minimum. To validate our results, tests were done on the basis set and the functional used. Single-point energy calculations were performed on all optimized structures using the triple basis set 6-311g* for all atoms. Similarly, different functionals, including pure DFT as the PBE functional[41] and hybrid DFT as the B3LYP[42] and PBE0[43] functionals, were tested. In addition, single-point energy calculations were performed in the acetone solvent with the polarized continuum model, CPCM.[44]

Results and Discussion

Fluorinated Ligand Synthesis. The synthesis of the fluorinated ligand F_2-HL_{CH_3} was carried out as follows via the procedure outlined in Figure 1. From commercially available 2-fluoro-6-methylpyridine, a controlled reaction with 2 equiv of NBS leads to the dibrominated compound **2** (75% yield). Conversion of **2** to the desired aldehyde **3** is accomplished by oxidation with $AgNO_3$ (60% yield). Upon addition of the 2-(aminomethyl)-pyridine to the aldehyde **3** and reduction, the corresponding nonsymmetric amine **4** is obtained (82% yield). Substitution of both chloride groups of 2,6-bis(chloromethyl)-4-methylphenol by 2 equiv of amine **4** provides the desired ligand (30% yield).

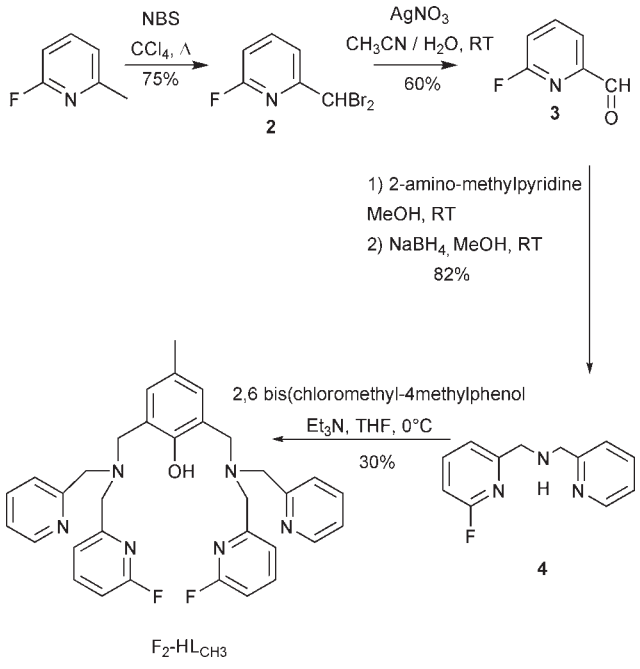

Figure 1. F_2-HL_{CH_3} ligand synthetic pathway.

The F_2-HL_{CH_3} ligand (Scheme 1b) has two different isomeric forms: one possesses a pseudo-mirror axis with the two tertiary amines in opposite configurations ($R-S$ or $S-R$), and the other possesses a pseudo-two-fold axis with the two tertiary amines in the same configuration ($R-R$ or $S-S$). It should be emphasized that, in the free ligand, fast inversion of the nitrogen atoms of the amine arms interconverts the two possible isomeric forms. When each amine nitrogen is bound to a copper atom, the two geometric isomers could potentially be obtained.

(39) Becke, A. D. *Phys. Rev. A* **1988**, *38*, 3098.
(40) Lee, C.; Yang, W.; Parr, R. C. *Phys. Rev. B* **1988**, *37*, 785.
(41) Perdew, J. P.; Burke, K.; Ernzerhof, M. *Phys. Rev. Lett.* **1997**, *78*, 1396.
(42) Adamo, C.; Barone, V. *J. Chem. Phys.* **1999**, *110*, 6158.
(43) Becke, A. D. *J. Chem. Phys.* **1993**, *98*, 5648.
(44) Cossi, M.; Scalmani, G.; Rega, N.; Barone, V. *J. Chem. Phys.* **2002**, *117*, 43.

Table 2. Bond Lengths (Å) and Bond Angles (°) in the Cationic Units for $\mathbf{1}_{meso}$ and $\mathbf{1}_{rac}$ from X-ray Data and Theoretical Results (in Italics)

$\mathbf{1}_{meso}\cdot 3C_4H_8O$ (From CH_3CN/THF)			$\mathbf{1}_{rac}\cdot CH_3CN$ (From CH_3CN/H_2O)		
	expt	*calcd*		expt	*calcd*
Cu1−O1	1.959(3)	*2.02*	Cu1− O1	1.978(2)	*2.05*
Cu1−O2	1.900(3)	*1.96*	Cu1 −O2	1.905(2)	*1.96*
Cu1−N1	2.018(3)	*2.04*	Cu1 −N1	2.010(3)	*2.03*
Cu1−N3	2.238(4)	*2.17*	Cu1− N3	2.125(3)	*2.13*
Cu1−N4	1.992(3)	*2.00*	Cu1− N4	2.014(3)	*2.07*
Cu2−O1	2.019(3)	*2.06*	Cu2 −O1	1.954(2)	*2.03*
Cu2−O2	1.890(3)	*1.96*	Cu2− O2	1.901(2)	*1.95*
Cu2−N2	2.006(3)	*2.04*	Cu2− N2	2.012(3)	*2.05*
Cu2−N5	2.115(3)	*2.11*	Cu2 −N5	1.988(3)	*2.03*
Cu2−N6	2.042(3)	*2.04*	Cu2− N6	2.205(3)	*2.14*
Cu1−O1−Cu2	96.9(1)	*99.7*	Cu1−O1−Cu2	98.1(1)	*98.7*
Cu1−O2−Cu2	103.5(1)	*105.2*	Cu1−O2−Cu2	102.6(1)	*105.2*
O1−Cu1−O2	80.4(1)	*78.0*	O1−Cu1−O2	79.2(1)	*77.7*
O1−Cu1−N1	91.1(1)	*92.0*	O1−Cu1−N1	91.4(1)	*91.4*
O1−Cu1−N3	105.0(1)	*108.8*	O1−Cu1−N3	113.5(1)	*117.7*
O1−Cu1−N4	148.1(1)	*136.7*	O1−Cu1−N4	127.2(1)	
O2−Cu1−N1	169.3(1)	*166.9*	O2−Cu1−N1	170.6(1)	
O2−Cu1−N3	109.4(1)	*110.7*	O2−Cu1−N3	103.6(1)	
O2−Cu1−N4	99.0(1)	*96.8*	O2−Cu1−N4	101.3(1)	
N1−Cu1−N3	79.0(1)	*136.7*	N1−Cu1−N3	80.7(1)	
N1−Cu1−N4	84.8(1)	*80.3*	N1−Cu1−N4	83.7(1)	
N3−Cu1−N4	105.3(1)	*113.0*	N3−Cu1−N4	117.4(1)	
O1−Cu2−O2	79.1(1)	*136.7*	O1−Cu2−O2	79.8(1)	
O1−Cu2−N2	92.2(1)	*92.4*	O1−Cu2−N2	91.8(1)	
O1−Cu2−N5	117.4(1)	*117.8*	O1−Cu2−N5	135.6(1)	
O1−Cu2−N6	123.5(1)	*122.9*	O1−Cu2−N6	107.0(1)	
O2−Cu2−N2	169.8(1)	*169.4*	O2−Cu2−N2	171.6(1)	
O2−Cu2−N5	106.3(1)	*103.8*	O2−Cu2−N5	100.8(1)	
O2−Cu2−N6	98.1(1)	*100.2*	O2−Cu2−N6	104.0(1)	
N2−Cu2−N5	82.4(1)	*83.1*	N2−Cu2−N5	84.4(1)	
N2−Cu2−N6	82.1(1)	*83.3*	N2−Cu2−N6	79.2(1)	
N5−Cu2−N6	117.3(1)	*118.0*	N5−Cu2−N6	115.5(1)	

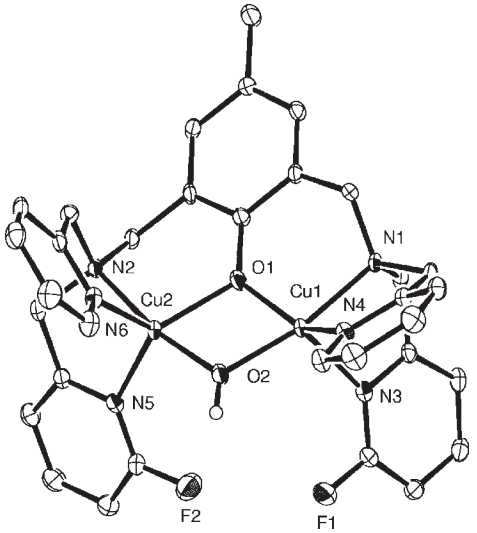

Figure 2. ORTEP view of the cation of $[Cu_2(C_{33}H_{31}F_2ON_6)(\mu\text{-OH})](ClO_4)_2\cdot 3C_4H_8O$ ($\mathbf{1}_{meso}\cdot 3C_4H_8O$). Ellipsoids drawn at 30% probability. Hydrogen atoms are omitted for clarity, except for the hydroxo group.

Synthesis and Characterization of the Dinuclear Copper(II) Complex. From the fluorinated ligand F_2-HL_{CH_3} (Scheme 1b), the corresponding μ-phenoxo,μ-hydroxo dicopper complex was prepared by standard procedures[16] and characterized. Two equivalents of $Cu^{II}(ClO_4)_2\cdot 6H_2O$ was reacted with a solution of ligand in acetonitrile containing 2 equiv of triethylamine. The dark green solid that precipitated upon addition of THF is the dinuclear complex **1**, in which $\mathbf{1}^{2+}$ corresponds to the $[Cu_2(F_2\text{-}L_{CH_3})(\mu\text{-OH})]^{2+}$ cation. The ^{19}F NMR spectrum (see below) shows the presence of two species.

Description of Crystal Structures. The unique feature of complex **1** became clearly apparent upon X-ray crystallographic analysis. Crystallization of complex **1** was first carried out using a CH_3CN/THF solution at −20 °C over 2 days, allowing isolation of an isomeric form, namely $\mathbf{1}_{meso}$. The isomerism is determined by the disposition of the fluorine atoms with respect to the plane containing the Cu_2O_2 core. For $\mathbf{1}_{meso}$, both fluorine groups are oriented on the same side. Crystal structure parameters are given in the Experimental Section. An ORTEP view of the cationic complex is shown in Figure 2. Selected bond lengths and angles are given in Table 2.

Crystals of $[Cu_2(C_{33}H_{31}F_2ON_6)(\mu\text{-OH})](ClO_4)_2\cdot 3C_4H_8O$ ($\mathbf{1}_{meso}\cdot 3C_4H_8O$) contain three associated solvent molecules and are stable if coated with THF. Without protection, the facile efflorescence of the solvent molecule results in the decomposition of the crystals within 30 min at ambient temperature. The complex $\mathbf{1}_{meso}\cdot 3C_4H_8O$ is structurally very similar to the $[Cu_2(L_{CH_3})(\mu\text{-OH})](ClO_4)_2\cdot 0.5C_4H_8O$ and $[Cu_2(L_{OCH_3})(\mu\text{-OH})](ClO_4)_2\cdot C_4H_8O$ complexes, which differ from the $[Cu_2(L_F)(\mu\text{-OH})](ClO_4)_2$ complex.[16,30] All of these complexes crystallize in different space groups, with different cell parameters and different numbers of solvent molecules. However, the cationic complexes have the same molecular arrangement. Furthermore, the $\mathbf{1}_{meso}$ complex possesses a pseudo-mirror axis with the two tertiary amines in opposite configurations. As the space group is centrosymmetric, both the $R-S$ and $S-R$ configurations are observed. The crystal structure

reveals that the two copper atoms are doubly bridged by the phenoxo and a hydroxo group. Pentacoordination of Cu1 and Cu2 is achieved by the tertiary amine and two pyridine nitrogens. The coordination polyhedron of the Cu1 atom is best described as a square pyramid with N3 at the apex. The Cu1 atom is 0.35 Å from the square plane defined by O1, O2, N1, and N4 atoms. The coordination polyhedron of the Cu2 atom is best described as a distorted trigonal bipyramid. Cu2 is located 0.156 Å out of the basal plane defined by O1, N5, and N6 atoms, toward the O2 atom. The Cu−N and Cu−O distances are 1.99(2)−2.24(3) and 1.89(2)−2.02(2) Å, respectively, in the same ranges as in previously characterized complexes. The four atoms Cu1, Cu2, O1, and O2 are in the same plane, with a maximal deviation from the least-squares plane of 0.023(6) Å. Accordingly, the angles in the Cu_2O_2 unit are relatively close, leading to the short Cu1···Cu2 intermetallic distance (2.98(1) Å). The former is very similar to those observed in the other μ-phenoxo,μ-hydroxo copper(II) dimers (in the range of 2.966(1)−3.082(3) Å) with relevant ligands.[16,30,44] The phenolate ring is both tilted toward the O1−O2 axis and twisted with respect to the O1−Cu2−O2−Cu1 plane.

The tilting is observed by measuring the angle O2−O1−C1 (158.7(3)°) and the twisting from the torsion angles Cu1−O1−C1−C2 and Cu2−O1−C1−C6 (respectively, 2.9(5)° and −37.4(5)°). Therefore, Cu1, Cu2, and O2 lie on the same side of the phenoxo plane (O1, C1, C2, C3, C4, C5, C6). A hydrogen bond is established between the hydroxo and the O5 oxygen atom of the perchlorate ion (O2−H···O5) with d(O2···O5) = 2.87(3) Å.

By using slow crystallization conditions, we were able to obtain another geometric isomer of **1** (Figure 3). Crystals of the isomer $\mathbf{1}_{rac}$ were observed after 6 weeks of slow evaporation of **1**, dissolved in a CH_3CN/H_2O mixture at room temperature. The structure of $[Cu_2(C_{33}H_{31}F_2ON_6)(\mu\text{-OH})](ClO_4)_2\cdot CH_3CN$ ($\mathbf{1}_{meso}\cdot CH_3CN$) also contains associated solvent molecules; however, decomposition of the crystals after air exposure is not observed. The major difference between the $\mathbf{1}_{rac}$ complex and the $\mathbf{1}_{meso}$ complex is the spatial arrangement of the pyridines bearing a fluorine atom *trans* to each other. Complex $\mathbf{1}_{meso}$ possesses a pseudo-two-fold axis, leading to the same configuration for the two tertiary amines. As the space group is centrosymmetric, both the $R-R$ and $S-S$ configurations are observed in the crystal structure. Each copper atom is pentacoordinated to the tertiary amine, two pyridine nitrogen atoms, the oxygen of the phenoxo bridge, and an oxygen atom of the hydroxo bridge.

The coordination polyhedra around Cu1 and Cu2 are mainly distorted trigonal bipyramids. Axial positions are occupied respectively by N1 and O2 for Cu1 and by O2 and N2 for Cu2. For Cu1, the trigonal plane is defined by the N3, N4, and O1 atoms, with a mean deviation from the plane of 0.16 Å for the copper atom. The Cu2 center lies 0.15 Å out of the trigonal plane (N5, N6, O1 atoms). The longest distances, Cu1−N3 (2.125(3) Å) and Cu2−N6 (2.205(3) Å), from the fluorinated pyridines are in the same range as those previously characterized for $\mathbf{1}_{meso}$. By comparison with the former complex, the pentacoordinated copper centers display very similar Cu−N bonds in the range of 1.988(3)−2.205(3) Å and slightly shorter Cu−O bond lengths, 1.901(2)−1.978(2) Å. The angles

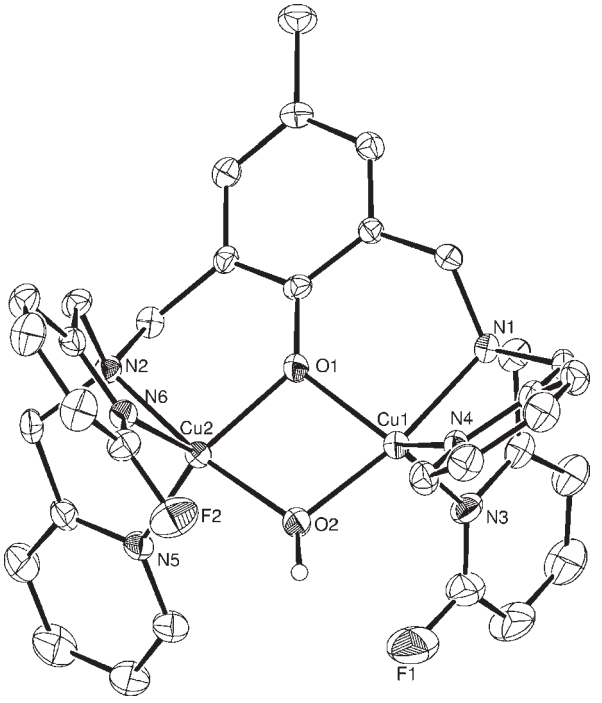

Figure 3. ORTEP view of the cation of $[Cu_2(C_{33}H_{31}F_2ON_6)(\mu\text{-OH})](ClO_4)_2\cdot CH_3CN$ ($\mathbf{1}_{rac}\cdot CH_3CN$). Ellipsoids drawn at 30% probability. Hydrogen atoms are omitted for clarity, except for the hydroxo group.

in the Cu_2O_2 unit are almost the same as those observed in $\mathbf{1}_{meso}$; the differences are less than 1.2°, whereas the mean distances Cu−O in the Cu_2O_2 unit are shorter. This leads to an intermetallic distance Cu1···Cu2 of 2.9070(5) Å, one of the shortest distances observed for a doubly bridged (phenoxo and hydroxo) dicopper complex.[16,30,45]

Following crystallization of another batch using a CH_3CN/H_2O solution over 2 months, another related form, $\mathbf{1'}_{rac}$, was isolated. (See Figure S1 and crystal description in the Supporting Information.)

In all structures, the spatial disposition of the pyridine groups relative to each other around the copper atoms makes the metal site rather accessible (see another drawing of $\mathbf{1}_{meso}$, $\mathbf{1}_{rac}$, and $\mathbf{1'}_{rac}$, Figure S2 in the Supporting Information). In complex $\mathbf{1}_{meso}$, the F1···F2 distance is short (2.82 Å). In contrast, the fluorine distances in $\mathbf{1}_{rac}$ and $\mathbf{1'}_{rac}$ (5.848 and 5.943 Å, respectively; see Supporting Information) are larger, minimizing steric and/or electronic interactions between the two fluorine atoms.

Solution Studies. In acetone, the ESI mass spectra of complexes $\mathbf{1}_{meso}$ and $\mathbf{1}_{rac}$ show similar behavior, with a peak at m/z = 809 (z = 1) corresponding to the $[Cu_2(C_{33}H_{31}F_2ON_6)(OH)](ClO_4)]^+$ ion. (Figures S3 and S4 in the Supporting Information show the observed/theoretical isotopic pattern distribution.) These data provide evidence that the dibridged dimeric copper(II) structure remains in solution.

General UV−vis features for dicopper(II) complexes in acetone are depicted in Table 3. All complexes are characterized by a ligand-to-metal charge-transfer (LMCT) transition between the bridging phenoxo and copper ions in the 400−450-nm region and a d−d transition in the 650−790-nm region. These transitions are affected to a

(45) Maloney, J. J.; Glogowski, M.; Rohrbach, D. F.; Urbach, F. L. *Inorg. Chim. Acta* **1987**, *127*, L33.

Table 3. Selected Properties for Fluorinated Ligands and Related Cationic Dicopper Complexes: $[Cu_2(L_{CH_3})(\mu\text{-OH})]^{2+}$, $[Cu_2(L_F)(\mu\text{-OH})]^{2+}$, $\mathbf{1_{meso}}$, and $\mathbf{1_{rac}}$

	UV−vis, λ_{max}/nm (ε/$M^{-1}cm^{-1}$)[a]		^{19}F NMR parameters	
compound	LMCT	d−d	δF (ppm)[b]	$\Delta\nu_{1/2}$(Hz)[c]
ligand F_2-HL_{CH_3}			93.7	15.5
ligand HL_F			32.0	11
$[Cu_2(L_{CH_3})(\mu OH)]^{2+}$ [16]	410 (480)	785 (280)		
$[Cu_2(L_F)(\mu\text{-OH})]^{2+}$ [30]	410 (440)	781 (260)	39.9	60
$\mathbf{1_{meso}}$	410 (sh)	774 (240)	120.2	502
$\mathbf{1_{rac}}$	446 (864)	657 (132)	96.3	192

[a] Acetone solution (1.25×10^{-4} M at 25 °C). [b] Observed chemical shifts in ppm relative to C_6F_6. [c] Line width.

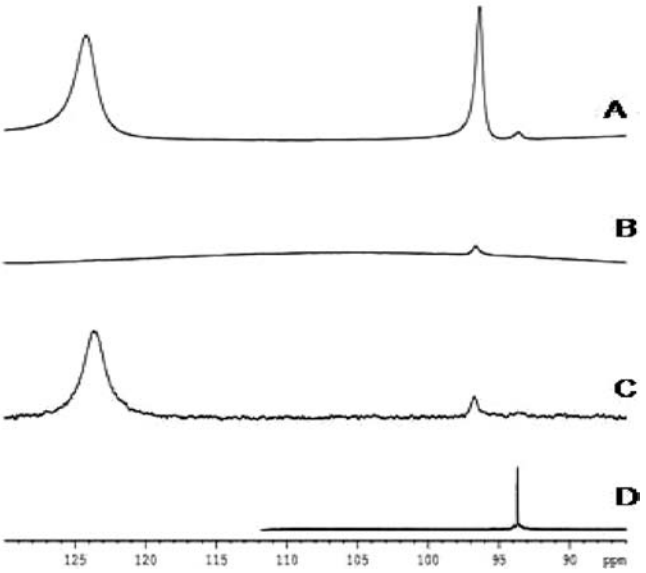

Figure 4. ^{19}F NMR spectra (282.4 MHz, 323 K, ppm vs C_6F_6 in acetone-d_6): (A) **1** as crude powder after immediate dissolution and recording, (B) $\mathbf{1_{rac}}\cdot CH_3CN$ crystal recovered from X-ray structure determination after immediate dissolution and recording, (C) crystals of $\mathbf{1_{meso}}$ coated by THF after immediate dissolution and recording, and (D) the ligand F_2-HL_{CH_3}.

lesser extent by the electronic features of the substituent on the phenolic group, while the electron-withdrawing fluorinated groups on pyridines induce significant shifts. The position of the d−d bands (774 and 657 nm for $\mathbf{1_{meso}}$ and $\mathbf{1_{rac}}$, respectively) is particularly affected by the geometric modifications around the copper(II) centers. These differences suggest different coordination geometry around the copper ions for $\mathbf{1_{meso}}$ and $\mathbf{1_{rac}}$ compounds in acetone solution.

^{19}F NMR has been used successfully for studies on paramagnetic dicopper complexes[30,31] and may be an interesting tool to study the behavior in solution of the fluorinated compounds described herein. In particular, the two well-separated signals (δ_F = 120.2 and 96.4 ppm, Figure 4A) observed in the crude complex **1** spectrum after immediate dissolution and recording in acetone-d_6 indicated the presence of two species in solution in almost equal amounts. The signal at 96.3 ppm is assigned to the *trans* isomer, based on the similar chemical shift observed in the ^{19}F NMR spectrum in acetone-d_6 of the crystal used for X-ray structure determination of $\mathbf{1_{rac}}$ (Figure 4B) after dissolution and immediate recording.

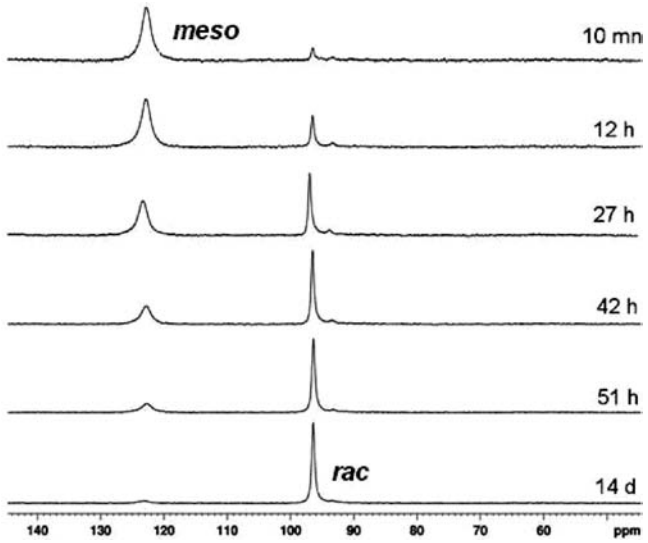

Figure 5. Solution isomerization evidenced by ^{19}F NMR (282.4 MHz, 323K, ppm vs C_6F_6 in acetone-d_6) spectra of $\mathbf{1_{meso}}$ recorded after immediate dissolution in acetone-d_6 and over time, showing the formation of $\mathbf{1_{rac}}$.

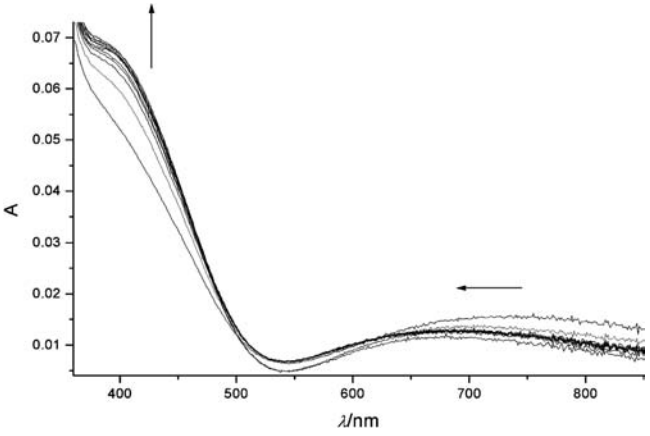

Figure 6. UV−vis spectra of $\mathbf{1_{meso}}$ (1.55×10^{-4} M, 25 °C) after immediate dissolution in acetone and over time during 14 days, showing the formation of $\mathbf{1_{rac}}$.

The ^{19}F NMR spectrum of $\mathbf{1_{meso}}$ crystals after dissolution and immediate recording in acetone-d_6 (Figure 4C) exhibits a predominant signal at 120.2 ppm, assigned to the isomer $\mathbf{1_{meso}}$, and a signal at 96.4 ppm beginning to emerge with time, indicating a *meso*−*rac* isomerization process in solution. The small signal observed at 93.5 ppm (Figure 4A) corresponds to the free ligand (Figure 4D). General ^{19}F NMR features for paramagnetic dicopper(II) complexes and related ligands are collected in Table 3. Remarkable differences regarding hyperfine shifts and larger signal width are evidenced. ^{19}F signals are very sensitive to the local environment (structural and magnetic)[29] in this series of dicopper(II) complexes.[30] The observed differences in behavior toward ^{19}F NMR for $\mathbf{1_{rac}}$ and $\mathbf{1_{meso}}$ isomers demonstrate that ^{19}F NMR discriminates the two isomers and provides the clearest evidence of the presence of the two isomeric forms in solution.

Isomerization of $\mathbf{1_{meso}}$ in Solution. Crystals of $\mathbf{1_{meso}}$ were dissolved in acetone-d_6, and the corresponding ^{19}F NMR spectrum was recorded immediately after dissolution

Table 4. Computed Electronic Energies (in Hartrees) and DFT Spin Expectation Values $\langle S^2_{BS}\rangle$ for All Structures[a]

	$\mathbf{1_{meso}}$				$\mathbf{1_{rac}}$				$\mathbf{1_{rac}}$ vs $\mathbf{1_{meso}}$
method	$E_{S=1}$	E_{BS}	$\langle S^2_{BS}\rangle$	$E_{S=0}$	$E_{S=1}$	E_{BS}	$\langle S^2_{BS}\rangle$	$E_{S=0}$	$\Delta E_{S=0}$
BLYP 6-31 g*	−5235.129629	−5235.133506	0.7561	−5235.135863	−5235.126570	−5235.135862	0.7371	−5235.141187	3.3
BLYP/CPCM 6-31 g*	−5235.312560	−5235.317107	0.8022	−5235.320152	−5235.311885	−5235.317508	0.7468	−5235.320859	0.5
BLYP 6-311 g*	−5235.912172	−5235.917024	0.6910	−5235.919586	−5235.910421	−5235.918730	0.6289	−5235.922541	1.9
B3LYP 6-31 g*	−5235.755791	−5235.758517	0.9773	−5235.761123	−5235.755627	−5235.756611	0.9692	−5235.757535	−2.2
PBE 6-31 g*	−5232.851689	−5232.852956	0.7170	−5232.853664	−5232.846796	−5232.854769	0.7162	−5232.859216	3.5
PBE0 6-31 g*	−5232.995133	−5233.015211	0.9838	−5233.034649	−5232.993626	−5233.013128	0.9812	−5233.031910	−1.7

[a] All calculations were performed using the broken-symmetry geometries which were optimized at the BLYP/6-31g* level of theory. Relative electronic energies for the singlet state $\Delta E_{S=0}$ (in kcal mol^{-1}) are given with $\Delta E_{S=0} = E_{S=0}(meso) - E_{S=0}(rac)$.

(Figure 4C). The predominant resonance at 120.2 ppm was assigned to the $\mathbf{1_{meso}}$ isomer, and the minor resonance at 96.4 ppm was assigned to the isomer $\mathbf{1_{rac}}$ (see discussion above).

The decrease in intensity of the signal at 120.2 ppm with time is concomitant with the increase of the signal at 96.4 ppm, suggesting the conversion of *meso* to *rac* isomers (Figure 5). The *meso:rac* ratio appeared to reach an equilibrium in acetone-d_6 after some days. An approximate estimation of the *meso:rac* ratio from ^{19}F NMR integration signals as a function of time is given in Supporting Information (Figure S5). The solvent dependence (acetone vs acetonitrile; Supporting Information, Figure S6) of the isomerization process has been also studied (Supporting Information, Figure S7). The observed conversion of the *meso* to *rac* isomers in solution is probably due to the minimized interaction effects between the two fluorine atoms in $\mathbf{1_{rac}}$, leading to the formation of the most thermodynamically stable isomer.

The UV−vis spectrum of $\mathbf{1_{meso}}$ in acetone is characterized by two absorbance features at 410 and 774 nm. Over time, the absorbance at 410 nm increases, with a slight bathochromic shift at 445, while the absorbance at 774 nm displays a hypsochromic shift at 659 nm (Figure 6). The spectrum obtained after 1 month was close to the UV−vis features obtained from isolated $\mathbf{1_{rac}}$ compound, supporting the slow *meso:rac* isomerization in acetone solution (see above). Nevertheless, the slight variations observed in the UV−vis spectra were insufficient to be considered as direct evidence of the isomerization process and to be used to estimate the *meso:rac* ratio as a function of time compared to the more accurate ^{19}F NMR data.

DFT Calculations of $\mathbf{1_{meso}}$ and $\mathbf{1_{rac}}$ Structures. DFT calculations were performed to confirm the formation of the two isomers. From a theoretical point of view, the complicated electronic structures of the two isomers containing a Cu_2O_2 core are particularly interesting. The presence of two magnetically coupled Cu^{II} ions with their formal d^9 electronic configuration gives rise to exchange coupling phenomena, leading to either a singlet or a triplet state. DFT methods have been widely employed for studying such systems, and the reliability of the results has been extensively discussed.[34−36] One common issue lies in the monodeterminental nature of the DFT, but it can be bypassed using the unrestricted broken-symmetry approach.[46,47] Another issue is how to account for both dynamic and nondynamic parts of the electron correlation effects in the treatment of such molecules. Cramer et al.[35] have shown that pure DFT functionals could provide accurate predictions for Cu_2O_2 systems with ligands as large as in our systems. For these reasons, all calculations were carried out with the BLYP functional. First, we performed a geometric optimization of both isomers in their triplet and broken-symmetry states. The broken-symmetry state of $\mathbf{1_{rac}}$ ($\mathbf{1_{meso}}$) was found to have an electronic energy 2.7 kcal mol^{-1} (1.1 kcal mol^{-1}) lower than that of the triplet state. These results show that each isomer features an antiferromagnetic coupling, so that the singlet state is the ground spin state for both systems. These data are experimentally supported by EPR (silent spectrum for complex **1**).

Thus, all of the following calculations were performed using the geometries optimized in the broken-symmetry state. The main bond lengths and angles observed in the crystallographic structures are listed in Table 2, along with the theoretical values obtained from the broken-symmetry optimizations. From this table, we observe that the difference between the calculated and experimental bond lengths never exceeds ±0.07 Å. Finally, the energies of the pure singlet states were computed using the spin-projection method:[48]

$$E_{S=0} = \frac{2E_{BS} - \langle S^2_{BS}\rangle E_{S=1}}{2 - \langle S^2_{BS}\rangle}$$

where all the energies are given for the broken-symmetry geometry, and $\langle S^2_{BS}\rangle$ is the spin-expectation value of the broken-symmetry calculation. In Table 4, we report the computed relative electronic energies for all structures along with the corresponding $\langle S^2_{BS}\rangle$ values.

From this table, it can be seen that the experimental trend is well reproduced by our theoretical calculations. First, the electronic energies of the two isomers are very close to each other, which may explain the formation of the two forms. Second, the energy balance tends to favor the *rac* conformation, in agreement with the isomerization of $\mathbf{1_{meso}}$ in acetone solution. The singlet state of $\mathbf{1_{rac}}$ has an electronic energy 3.3 kcal mol^{-1} lower than that of the singlet state of $\mathbf{1_{meso}}$. Solvent calculations using a polarized continuum model[44] gave similar results. However, because the energy differences between the *meso* and *rac* isomers were at the accuracy limit of the method, additional calculations employing various functionals and basis sets were performed. The results are summarized in Table 4. Values obtained using a basis set of

(46) Noodleman, L. *J. Chem. Phys.* **1981**, *74*, 5737.
(47) Noodleman, L.; Davidson, E. R. *Chem. Phys.* **1986**, *109*, 131.
(48) Yamaguchi, K.; Jensen, F.; Dorigo, A.; Houk, K. N. *Chem. Phys. Lett.* **1988**, *149*, 537.

double- or triple-ζ quality are fairly similar. Our results show that all the functionals used give electronic relative energies in the same range. These values justify the formation of the two geometric isomers $\mathbf{1}_{meso}$ and $\mathbf{1}_{rac}$ during the complexation of two copper(II) ions by our new ligand F_2-HL_{CH_3}. Finally, in agreement with the results obtained by Cramer et al.,[35] we found that for these systems the pure BLYP or PBE DFT functionals perform better than the B3LYP or PBE0 hybrid functionals. Only pure DFT functionals could reproduce the experimental trend that the $\mathbf{1}_{rac}$ isomer is the most thermodynamically stable isomer.

Conclusions

Efficient fluorine labeling has been accomplished, allowing the separation of two geometrical forms after copper(II) complexation, as shown in both solid and solution states. Complex **1** exists as *meso:rac* geometric isomers due to a possible rotation of the pyridine arms. Rapid crystallization of complex **1** allows isolation of the kinetic *meso* isomeric form, while slow crystallization makes it possible to obtain *rac* isomers ($\mathbf{1}_{rac}$ and $\mathbf{1'}_{rac}$).

Combined UV−vis and ^{19}F NMR solution studies lead to the conclusion that in acetone the kinetic *meso* isomer of **1** undergoes conversion to the corresponding thermodynamic *rac* form via a dissociative process. The stability of *rac* isomers can be explained by the arrangement preventing interaction of the fluorine groups. These features could be important for further steps in catalytic processes or in binding studies on such dinuclear complexes. From this study and previous research,[29] it is clear that ^{19}F NMR is ideally suited for the study of such subtle changes in solution, such as geometric isomerism from paramagnetic dinuclear complexes.

Finally, theoretical calculations were performed on these systems and corroborated the experimental results. This study supports the idea that the use of pure DFT functionals as BLYP or PBE functionals for modeling the complicated electronic structure of dinuclear copper(II) complexes renders quantitatively correct results.

Acknowledgment. The authors thank the French Agence Nationale pour la Recherche for financial support (ANR-09-BLAN-0028-01) and for the M.O. grant. We are grateful to Béatrice Genaro (DCM) and Sylvette Beynes (DCM) for assistance on NMR studies, Corinne Bailly (DCM) for help in X-ray determinations, and Bernard Brasme (ICMG) for measuring ESI-MS spectra.

Supporting Information Available: Crystal data; ORTEP views for $\mathbf{1'}_{rac} \cdot H_2O$ and cations $\mathbf{1}_{meso}$, $\mathbf{1}_{rac}$, and $\mathbf{1'}_{rac}$; ESI-MS data; ^{19}F NMR spectra in acetonitrile or acetone; plots of $\mathbf{1}_{meso}/\mathbf{1}_{rac}$ ratio from ^{19}F NMR as a function of time in acetone or acetonitrile; Cartesian coordinates of the optimized geometries in the broken symmetry states obtained using the BLYP functional and the basis set 6-31g*; X-ray crystallographic data, in CIF format, for $\mathbf{1}_{meso}$, $\mathbf{1}_{rac}$, and $\mathbf{1'}_{rac}$. This material is available free of charge via the Internet at http://pubs.acs.org.